

High bias transport and magnetometer design in open quantum dots

M. Switkes, A. G. Huibers, and C. M. Marcus^{a)}
Department of Physics, Stanford University, Stanford, California 94305

K. Campman and A. C. Gossard
Materials Department, University of California, Santa Barbara, California 93106

(Received 25 August 1997; accepted for publication 21 November 1997)

We report transport measurements as a function of bias in open semiconductor quantum dots. These measurements are well described by an effective electron temperature derived from Joule heating at the point contacts and cooling by Wiedemann-Franz out-diffusion of thermal electrons. Using this model, we propose and analyze a quantum dot based sensor capable of measuring absolute magnetic field at micron scales with a noise floor of ~ 110 nT/ $\sqrt{\text{Hz}}$ at 300 mK. Non optimized measurements reported here are ~ 2 orders of magnitude above this floor. © 1998 American Institute of Physics. [S0003-6951(98)00904-8]

Quantum dots have been studied extensively as controllable systems in which quantum phenomena can be probed with transport measurements.¹ Most experiments are performed at low bias, typically less than 20 μV for dots with total conductance $g \geq e^2/h$ ("open" dots), however many proposed applications will require higher bias to produce easily measurable signals. Experiments in quantum dots in the tunneling regime ($g \ll e^2/h$) have exploited the nonlinear conduction of quantum dots at high bias for energy level spectroscopy.² In open dots, conduction remains essentially linear, and the primary effect of the increased bias is to heat the electrons in the dot. In a quantum dot sensor, the optimum bias is a balance between increased signal from high bias and loss of quantum interference and increased noise from the elevated electron temperature. In this letter, we present measurements of high bias transport in open quantum dots in thermal equilibrium, and show that the data are well described by an effective electron temperature. We then apply this effective temperature model to a quantum dot magnetometer, using this result to investigate optimal design parameters, and compare it to alternative technologies for micron scale magnetometry.

The measurements were made in a ³He cryostat over a temperature range 340 mK–1.5 K with a quantum dot of area $A = 4.0 \mu\text{m}^2$ (Fig. 1 inset) defined by electron beam lithography on a GaAs/AlGaAs heterostructure using Cr/Au gates 160 nm above the two-dimensional electron gas (mobility $\mu = 1.2 \times 10^6 \text{ cm}^2/\text{V s}$ and density $n_s = 1.8 \times 10^{11} \text{ cm}^{-2}$). We measured conductance, $g = I_{\text{bias}}/V$, as a function of magnetic field B , cryostat temperature T_0 , and rms current bias I_{bias} , in two different configurations. The first configuration ("a" in Fig. 2 upper inset) used standard current-biased ac lock-in techniques at 200 Hz to measure g at several cryostat temperatures with I_{bias} fixed at 0.5 nA, small enough not to affect transport ($I_{\text{bias}} = 0.5$ and 1 nA give identical results at base temperature). The second configuration ("b" in Fig. 2 upper inset) measured g for several values of I_{bias} at $T_0 = 340$ and 580 mK using lock-in detection of a 43 Hz square wave excitation.

Figure 1 shows measurements of $g(B, T_0 = 340 \text{ mK},$

$I_{\text{bias}})$ along with the corresponding measurements of $g(B, T_0, I_{\text{bias}} = 0.5 \text{ nA})$. The close agreement of even the fine features of measurements made in these two configurations allows us to accurately assign an effective temperature, T_{eff} , to each bias current, shown in Fig. 2 for $T_0 = 340$ and 580 mK. This effective temperature can be interpreted as the electron temperature in the dot since inelastic electron-electron collisions, the primary thermalization mechanism in the temperature range of this experiment, occur at a rate³ $\tau_{ee}^{-1} = [\pi(k_B T)^2 / 4\hbar E_F] \ln(E_F / k_B T)$, which is comparable to or greater than the rate at which electrons escape from the dot, $\tau_D^{-1} = N\Delta / \pi\hbar$ where N is the number of open channels in each point contact, $\Delta = 2\pi\hbar^2 / m^* A$ is the mean spin-degenerate single-particle level spacing, and E_F is the Fermi energy. For our dot, $E_F = 6.3 \text{ meV}$, $N = 1$, and $\Delta = 1.8 \mu\text{eV}$, giving $\tau_D = 1.2 \text{ ns}$, $\tau_{ee} = 1.2 \text{ ns}$ at $T = 340 \text{ mK}$, and $\tau_{ee} = 0.17 \text{ ns}$ at $T = 1 \text{ K}$. While $\tau_{ee} \sim \tau_D$ at base temperature, as the effective temperature increases, τ_{ee} decreases, allowing the electrons to thermalize in the dot over most of the experimental range. This is in contrast to recent experi-

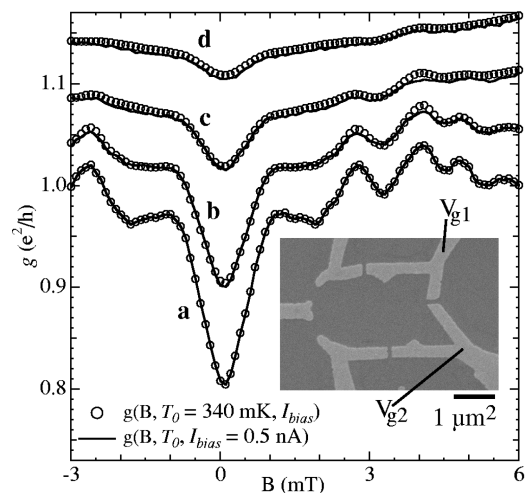


FIG. 1. Magnetoconductance, $g(B, T_0 = 340 \text{ mK}, I_{\text{bias}})$, for $I_{\text{bias}} = 0.5$ (a), 3 (b), 7 (c), and 12 nA (d) (open circles), with corresponding $g(B, T_0, I_{\text{bias}} = 0.5 \text{ nA})$ for $T_0 = 340$ (a), 410 (b), 680 (c), and 990 mK (d) (solid lines) showing the equivalence between bias and temperature. Each pair of curves has been offset for clarity. Inset: micrograph of measured device with shape distortion gates V_{g1} and V_{g2} labeled.

^{a)}Electronic mail: cmarcus@leland.stanford.edu

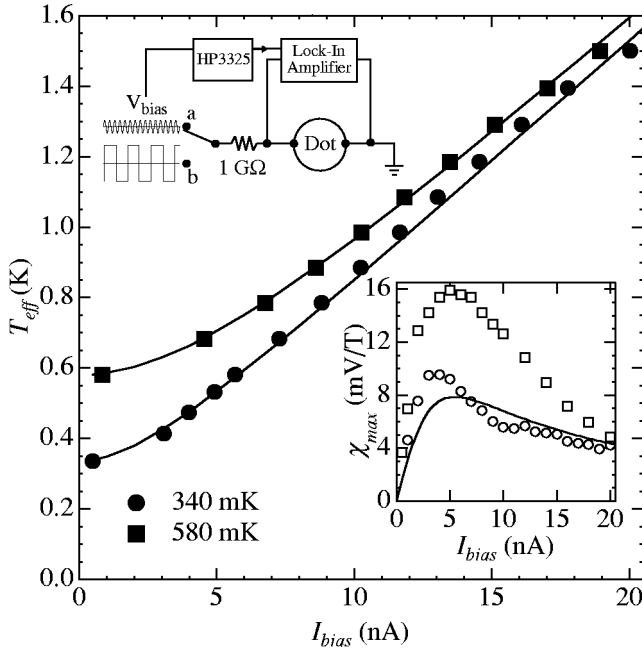


FIG. 2. Effective temperature, T_{eff} as a function of I_{bias} for $T_0 = 340$ and 580 mK (filled symbols) along with the theoretical value from Eq. (1) obtained by balancing Joule heating and Wiedemann-Franz cooling (solid lines). Upper inset: electrical schematic of the dot and measurement circuit for (a) low I_{bias} and (b) variable I_{bias} measurements. Lower inset: measurements of the voltage response χ_{max} at $T_0 = 340$ mK (open symbols) for two values of V_{g1} and V_{g2} along with the theoretical value for the ensemble-averaged voltage response $\langle \chi_{\text{max}} \rangle$ (solid line) which differs from measured values due to UCF.

ments by Linke and co-workers who found $T_{\text{eff}} = eV/k_B$ for electrons out of thermal equilibrium ($\tau_{ee} > \tau_D$), much higher than for thermalized electrons [Eq. (1)].⁴

The measured effective temperature can be quantitatively modeled by balancing the energy added to the dot by high bias electrons with the energy lost to the environment. The power input is Joule heating from the point contacts, $P_{\text{total}} = I_{\text{bias}}^2/g$. The heating occurs outside the point contact and is not necessarily evenly split between the dot and the lead⁵; as discussed below our data are best fit assuming $\sim 10\%$ asymmetry in heating. Cooling via the substrate is neglected since the electron-phonon scattering time⁶ is much longer than τ_D for all temperatures studied here. The main cooling mechanism is Wiedemann-Franz out diffusion of thermal electrons. Although originally developed for diffusive systems, the Wiedemann-Franz relation⁷ has been predicted⁸ and measured (to within a factor of 2)⁹ in ballistic point contacts. For our geometry (electrical resistance in series, thermal resistance in parallel), the Wiedemann-Franz relation gives a thermal conductivity $\sigma_{\text{th}} = 4gL_0T$, with the Lorenz number $L_0 = (k_B/e)^2 \pi^2/3$. Assuming that the reservoirs are in good thermal contact with the cryostat, this yields

$$T_{\text{eff}}^2 = T_0^2 + \frac{P_{\text{dot}}}{2gL_0}, \quad (1)$$

where P_{dot} is the power heating the dot which, for a symmetric point contact, is half of the total Joule power. We find best agreement with our data (as shown in Fig. 2) for $P_{\text{dot}} = 0.4P_{\text{total}}$. Presumably, the deviation of this coefficient from $1/2$ is due to asymmetry in the point contacts.⁵

The large magnetoconductance of a quantum dot around $B=0$ due to quantum-enhanced backscattering (weak localization) can be used to measure absolute magnetic field with spatial resolution on the order of the dot size. The effective temperature model can be used to help predict the performance of such a magnetometer and to select the optimum operating parameters. The device measured above was far from optimum with rms voltage noise $S_V^{1/2} \sim 150$ nV/ $\sqrt{\text{Hz}}$ referred to input, essentially independent of bias. This translates to a magnetic field noise $S_B^{1/2} = S_V^{1/2}/\chi \sim 10$ $\mu\text{T}/\sqrt{\text{Hz}}$ where $\chi \equiv dV/dB$ is the voltage response of the quantum dot. Approximately 20% of this noise is due to the amplifier and other extrinsic factors, and the rest is due to the dot itself.

If the dot noise is dominated by factors independent of bias, as is the case in this experiment, the maximum voltage response, $\chi = -(I_{\text{bias}}/g^2)dg/dB$, determines the best operating parameters. The *ensemble averaged*¹⁰ response can be calculated for a chaotically shaped ballistic dot from the Lorentzian line shape of the weak localization¹¹ $\langle g(B) \rangle = \langle g \rangle_{B \neq 0} - \langle \delta g \rangle / (1 + 4B^2/B_c^2)$, whose height¹² and width¹³ are, respectively, $\langle \delta g \rangle \equiv \langle g \rangle_{B \neq 0} - \langle g \rangle_{B=0} \sim (e^2/h)N / (2N + \gamma_\phi)$, and $B_c = \varphi_0^{(n)} \kappa^{1/2} (2N + \gamma_\phi)^{1/2}$, where $\langle g \rangle_{B \neq 0} = (e^2/h)N$ is the conductance at large magnetic field, $\varphi_0^{(n)} = 2\varphi_0 = h/e$ is the normal state magnetic flux quantum, $\kappa \propto A^{-5/2}$ is a constant of order 1 dependent on dot geometry, and $\langle \cdot \rangle$ indicates an ensemble-averaged quantity. Both $\langle \delta g \rangle$ and B_c depend on temperature through dephasing,¹⁴ which we have expressed in terms of the dimensionless rate $\gamma_\phi = 2\pi\hbar / (\Delta\tau_\phi)$. The low temperature ($340 \text{ mK} \leq T \leq 4 \text{ K}$) dephasing time, τ_ϕ , has recently been measured in similar devices for a range of dot areas from 0.4 to $4 \mu\text{m}^2$ with¹⁵ $\tau_\phi \sim [1.4T^2 \ln(73/T) + 13T]^{-1}$ for τ_ϕ in ns and T in K. Combining these equations and replacing T with T_{eff} yields the theoretical average voltage response $\langle \chi(B, T_0, I_{\text{bias}}) \rangle$ which has a maximum in magnetic field $\chi_{\text{max}} \equiv \chi(B_{\text{max}})$ at $B_{\text{max}} = B_c(1 - \langle \delta g \rangle / \langle g \rangle)^{1/2} / 2\sqrt{3}$. Two measurements of $\chi_{\text{max}}(T_0 = 340 \text{ mK}, I_{\text{bias}})$ for different values of the shape distorting gate voltages¹⁰ V_{g1} and V_{g2} (see Fig. 1 inset) are plotted in the lower inset of Fig. 2 along with the theoretical ensemble averaged value derived above, $\langle \chi_{\text{max}}(T_0 = 340 \text{ mK}, I_{\text{bias}}) \rangle$. The measured values differ from the ensemble averaged value due to universal conductance fluctuations (UCF) which remain in the unaveraged measurements.^{15,16} While this requires recalibration of the sensor for each value of V_{g1} and V_{g2} and for each thermal cycle, the UCF can be used to improve the response of the magnetometer by as much as a factor of 2 by ‘‘tuning’’ the dot with the shape distortion gates to a configuration with a high χ_{max} . In addition, since the voltage response is symmetric in magnetic field, $B=0$ is always indicated unambiguously. Figure 3a shows the theoretical $\langle \chi_{\text{max}} \rangle$ as a function of dot area and temperature for the bias (shown in Fig. 3b for $T_0 = 300$ mK) which yields the highest $\langle \chi_{\text{max}} \rangle$. If the noise is not dependent on the bias current, as in the experimental case, the maximum of this curve indicates the optimum operating bias.

The fundamental limit on noise of the quantum dot is set by the shot and Johnson-Nyquist noise which combine to give $S_V^{1/2} = \sqrt{4k_B T^*/g}$ with¹⁷ $T^* = T[1 + \alpha(eI_{\text{bias}}/2gk_B T) \coth(eI_{\text{bias}}/2gk_B T) - \alpha]$ where $\alpha = 1/4$ is the shot

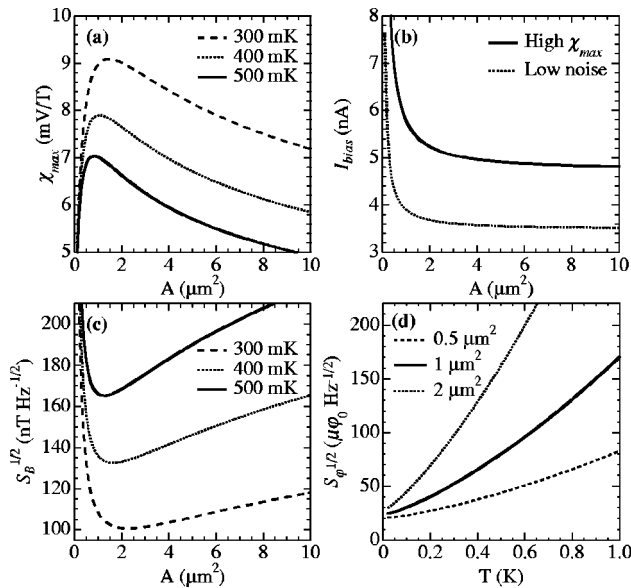


FIG. 3. Theoretical performance characteristics of the quantum dot magnetometer based on T_{eff} model: (a) Maximum voltage response $\langle \chi_{\max} \rangle$ as a function of dot area and temperature with I_{bias} chosen for greatest voltage response. (b) Bias current necessary for best voltage response (solid line) and lowest noise (broken line) at 300 mK. (c) Magnetic field noise $S_B^{1/2}$ with I_{bias} as shown in Fig. 3(b). (d) Magnetic flux noise $S_\phi^{1/2} = A S_B^{1/2}$.

noise suppression factor for quantum dots.¹⁸ In Fig. 3c, this noise is combined with the χ_{\max} calculated above and the resulting $S_B^{1/2}$ is shown as a function of dot area and cryostat temperature for the bias [shown in Fig. 3(b) for $T_0 = 300$ mK] which minimizes the noise. The noise in the measurements is far above this limit but could be greatly reduced by measuring at a frequency above the $1/f$ knee. See, for example, Ref. 17 where the authors have measured a point contact with a $1/f$ knee below 100 Hz.

Quantum dots compare favorably with other technologies for micron scale absolute magnetometry at millikelvin temperatures. While noise prevents the quantum dot measured here from being a competitive magnetic field sensor, improvements in the amplifiers and measuring frequency can yield a $1 \mu\text{m}^2$ dot with field noise $S_B^{1/2} \sim 100$ nT/ $\sqrt{\text{Hz}}$ [Fig. 3(c)]. This noise can be further reduced by as much as a factor of two by tuning shape distortion gates to improve the voltage response. Unfortunately, along with this tunability comes the necessity of calibrating the dot for each value of the shape distortion gates. This noise figure compares well to ~ 200 nT/ $\sqrt{\text{Hz}}$ for a submicron ballistic Hall probe.¹⁹ Both quantum dots and submicron hall bars have an order of magnitude higher flux noise than a state of the art commercial superconducting quantum interference device (SQUID),²⁰ ~ 6 nT/ $\sqrt{\text{Hz}}$ for a $1 \mu\text{m}^2$ device. Note, however, that the ultimate size limit for SQUIDs is the magnetic penetration length (~ 85 nm in Nb) whereas for devices based on chaotic quantum interference, the ultimate size limit is the Fermi wavelength which can be orders of magnitude smaller.

In conclusion, we have measured the effects of high bias on transport in open quantum dots and find that an effective temperature model balancing joule heating and Wiedemann-Franz heat conduction fits the data well. We use this model to establish performance limits for a magnetometer based on quantum dot technology, to suggest improvements toward achieving these limits, and compare them to alternative technologies.

The authors thank Dan Prober, Laurens Molenkamp, and Andrei Geim for very useful discussions. The authors gratefully acknowledge support at Stanford from the Office of Naval Research YIP program under Grant No. N00014-94-1-0622, the Army Research Office under Grant No. DAAH04-95-1-0331, the NSF-NYI program, the A. P. Sloan Foundation, and support for A.G.H. from the John and Fannie Hertz Foundation. We also acknowledge support at UCSB by the AFOSR under Grant No. 49620-94-1-0158.

- ¹C. W. J. Beenakker and H. Van Houten, in *Solid State Physics*, edited by H. Ehrenreich and D. Turnbull (Academic, San Diego, 1991), Vol. 44, p. 1; L. P. Kouwenhoven, C. M. Marcus, P. L. McEuen, S. Tarucha, R. M. Westervelt, and N. S. Wingreen, in *Proceedings of the Advanced Study Institute on Mesoscopic Electron Transport*, edited by L. P. Kouwenhoven, G. Schön, and L. L. Sohn (Kluwer, Dordrecht 1997).
- ²A. T. Johnson, L. P. Kouwenhoven, W. de Jong, N. C. van der Vaart, C. J. P. M. Harmans, and C. T. Foxon, *Phys. Rev. Lett.* **69**, 1592 (1992).
- ³L. Zheng and S. Das Sarma, *Phys. Rev. B* **53**, 9964 (1996).
- ⁴H. Linke, J. P. Bird, J. Cooper, P. Omling, Y. Aoyagi, and T. Sugano (to be published in *Phys. Rev. B* **56** (1997); for $T_{\text{eff}} \gg T_0$, the temperature derived from our heating model is about 0.2 eV/ k_B).
- ⁵M. Rokni and Y. Levinson, *Phys. Rev. B* **52**, 1882 (1995); V. L. Gurevich, *ibid.* **55**, 4522 (1997).
- ⁶A. Mittal, in *Quantum Transport in Semiconductor Submicron Structures*, edited by B. Kramer (Kluwer, Dordrecht, 1996), Vol. 326, p. 303.
- ⁷N. W. Ashcroft and N. D. Mermin, *Solid State Physics* (Saunders College, Philadelphia, 1976).
- ⁸C. R. Proetto, *Solid State Commun.* **80**, 909 (1991); A. Greiner, L. Reggiani, T. Kuhn, and L. Varani, *Phys. Rev. Lett.* **78**, 1114 (1997).
- ⁹L. W. Molenkamp, T. Gravier, H. van Houten, O. J. A. Buijk, M. A. A. Mabeoone, and C. T. Foxon, *Phys. Rev. Lett.* **68**, 3765 (1992).
- ¹⁰I. H. Chan, R. M. Clarke, C. M. Marcus, K. Campman, and A. C. Gossard, *Phys. Rev. Lett.* **74**, 3876 (1995).
- ¹¹H. U. Baranger, R. A. Jalabert, and A. D. Stone, *Phys. Rev. Lett.* **70**, 3876 (1993).
- ¹²H. U. Baranger and P. A. Mello, *Phys. Rev. B* **51**, 4703 (1995).
- ¹³R. M. Clarke, I. H. Chan, C. M. Marcus, C. I. Duruöz, J. S. Harris, Jr., K. Campman, and A. C. Gossard, *Phys. Rev. B* **52**, 2656 (1995).
- ¹⁴M. Büttiker, *Phys. Rev. B* **33**, 3020 (1986); C. M. Marcus, R. M. Westervelt, P. F. Hopkins, and A. C. Gossard, *ibid.* **48**, 2460 (1993).
- ¹⁵A. G. Huibers, M. Switkes, C. M. Marcus, K. Campman, and A. C. Gossard, *Cond-mat/9708170* (1997).
- ¹⁶R. L. Kautz, G. Zimmerli, and J. M. Martinis, *J. Appl. Phys.* **73**, 2386 (1993).
- ¹⁷A. Kumar, L. Saminadayar, D. C. Glatli, Y. Jin, and B. Etienne, *Phys. Rev. Lett.* **76**, 2778 (1996).
- ¹⁸R. A. Jalabert, J.-L. Pichard, and C. W. J. Beenakker, *Europhys. Lett.* **27**, 255 (1994).
- ¹⁹A. K. Geim, S. V. Dubonos, J. G. S. Lok, I. V. Grigorieva, J. C. Maan, L. T. Hansen, and P. E. Lindelof (unpublished); note that this noise floor is for a working Hall probe and may improve with further optimization.
- ²⁰Conductus, Inc., typical performance parameters of the S165c dc SQUID (1997).